International Journal of Nanomedicine

Dovepress
open access to scientific and medical research

Open Access Full Text Article

ORIGINAL RESEARCH

High UV-Vis-NIR Light-Induced Antibacterial Activity by Heterostructured TiO_2-FeS_2 Nanocomposites

This article was published in the following Dove Press journal:
International Journal of Nanomedicine

Chinmaya Mutalik,[1,*] Yu-Cheng Hsiao,[1,2,*] Yi-Hsuan Chang,[3] Dyah Ika Krisnawati,[4] Moh Alimansur,[4] Achmad Jazidie,[5,6] Mohammad Nuh,[7] Chia-Che Chang,[8] Di-Yan Wang,[8] Tsung-Rong Kuo[1,3]

[1]International PhD Program in Biomedical Engineering, College of Biomedical Engineering, Taipei Medical University, Taipei 11031, Taiwan; [2]Graduate Institute of Biomedical Optomechatronics, College of Biomedical Engineering, Taipei Medical University, Taipei 11031, Taiwan; [3]Graduate Institute of Nanomedicine and Medical Engineering, College of Biomedical Engineering, Taipei Medical University, Taipei 11031, Taiwan; [4]Dharma Husada Nursing Academy, Kediri, East Java 64114, Indonesia; [5]Department of Electrical Engineering, Institut Teknologi Sepuluh Nopember, Surabaya 60111, Indonesia; [6]Universitas Nahdlatul Ulama Surabaya, Surabaya 60111, Indonesia; [7]Department of Biomedical Engineering, Institut Teknologi Sepuluh Nopember, Surabaya 60111, Indonesia; [8]Department of Chemistry, Tunghai University, Taichung 40704, Taiwan

*These authors contributed equally to this work

Correspondence: Di-Yan Wang
Department of Chemistry, Tunghai University, Taichung 40704, Taiwan
Tel +886-4-23590121
Email diyanwang@thu.edu.tw

Tsung-Rong Kuo
Graduate Institute of Nanomedicine and Medical Engineering, College of Biomedical Engineering, Taipei Medical University, Taipei 11031, Taiwan
Tel +886-2-27361661
Email trkuo@tmu.edu.tw

Purpose: Antibiotic resistance issues associated with microbial pathogenesis are considered to be one of the most serious current threats to health. Fortunately, TiO_2, a photoactive semiconductor, was proven to have antibacterial activity and is being widely utilized. However, its use is limited to the short range of absorption wavelength.

Methods: In this work, heterostructured TiO_2-FeS_2 nanocomposites (NCs) were successfully prepared by a facile solution approach to enhance light-induced antibacterial activity over a broader absorption range.

Results: In TiO_2-FeS_2 NCs, FeS_2 NPs, as light harvesters, can effectively increase light absorption from the visible (Vis) to near-infrared (NIR). Results of light-induced antibacterial activities indicated that TiO_2-FeS_2 NCs had better antibacterial activity than that of only TiO_2 nanoparticles (NPs) or only FeS_2 NPs. Reactive oxygen species (ROS) measurements also showed that TiO_2-FeS_2 NCs produced the highest relative ROS levels. Unlike TiO_2 NPs, TiO_2-FeS_2 NCs, under light irradiation with a 515-nm filter, could absorb light wavelengths longer than 515 nm to generate ROS. In the mechanistic study, we found that TiO_2 NPs in TiO_2-FeS_2 NCs could absorb ultraviolet (UV) light to generate photoinduced electrons and holes for ROS generation, including $\cdot O_2^-$ and $\cdot OH$; FeS_2 NPs efficiently harvested Vis to NIR light to generate photoinduced electrons, which then were transferred to TiO_2 NPs to facilitate ROS generation.

Conclusion: TiO_2-FeS_2 NCs with superior light-induced antibacterial activity could be a promising antibacterial agent against bacterial infections.

Keywords: antibacterial agent, antibacterial mechanism, reactive oxygen species, light harvester, light-induced antibacterial activity

Introduction

The vigor and resistance of bacterial pestilences are growing day-by-day, and microbial infections are on the rise, creating serious hazards to human health worldwide. Antibiotic-resistant pathogenic infections can soon increase the mortality rate to millions each year.[1–5] A photoactive semiconductor, titanium dioxide (TiO_2), with economically feasible and biocompatible properties has shown unique antibacterial activity and has been in use for the past few decades.[6–8] TiO_2 was shown to be an effective antibacterial agent under ultraviolet (UV) light irradiation, by generating reactive oxygen species (ROS) which can cause irreparable damage to the cell envelope of microbes.[9–11] The effective generation of radicals such as H_2O_2, $\cdot OH$, and $\cdot O_2^-$ by TiO_2 is attributable to its reactivity to light, and it seems to be more efficient when doped or conjugated with other transition elements, noble metals, polymers, carbon, nitrogen, sulfur, or boron to form TiO_2 nanocomposites (NCs). TiO_2 NCs showed superior antibacterial activities to multidrug-resistant bacteria because of their ability to

efficiently absorb light and generation ROS.[12–20] The efficient light absorption of TiO_2 NCs can be ascribed to contracted bandgaps of TiO_2 due to the conjugation of inorganic and organic materials to TiO_2.[21–32]

To extend the absorption range, the NCs of iron disulfide (FeS_2) nanoparticles (NPs) conjugated with TiO_2 NPs (FeS_2-TiO_2 NCs) were synthesized. Recently, FeS_2-TiO_2 NCs were explored as a novel photocatalyst to harvest the light in the region from UV to near-infrared (NIR) for application in energy storage and conversion.[33] FeS_2 NPs with a small bandgap (~0.95 eV) have been utilized as efficient light harvesters to enhance the absorption from UV to NIR.[34] FeS_2-TiO_2 NCs also exhibited high photoelectric cell (PEC) performance for reducing CO_2 to methanol because the bandgap energy of FeS_2-TiO_2 NCs is narrowed to 1.70 eV for significant enhancement of the photocatalytic performance with visible (Vis) light irradiation.[35] Furthermore, TiO_2-FeS_2 NCs with photocatalytic applications in the UV-Vis-NIR region have shown great potential to be TiO_2-based photocatalysts in practical applications for highly active photocatalytic hydrogen evolution.[36] However, antibacterial applications with the use of photoactive, biocompatible, and low-cost TiO_2-FeS_2 NCs are still limited. The most pressing need is to combat wide bacterial infections in fields such as medicine, food, and water quality with the light-activated antibacterial agent of TiO_2-FeS_2 NCs.

In this work, light-driven catalysts of TiO_2-FeS_2 NCs were synthesized by a hydrothermal process and annealing method. Characterization studies were carried out to validate the structure and optics of TiO_2-FeS_2 NCs using scanning electron microscopy (SEM), transmission electron microscopy (TEM), powder x-ray diffraction (XRD), Raman spectroscopy, and UV-Vis-NIR spectrophotometry. Furthermore, antibacterial activities of TiO_2-FeS_2 NCs were investigated against *Escherichia coli* (*E. coli*) under illumination of simulated AM1.5 sunlight and in the dark. To study light-harvesting properties of FeS_2 NPs, the antibacterial efficiencies of TiO_2-FeS_2 NCs were also examined against *E. coli* under light irradiation with a 515-nm longpass filter. Moreover, to investigate details of the antibacterial mechanism, ROS generation of TiO_2-FeS_2 NCs against *E. coli* was measured before and after light irradiation.

Materials and Methods

Chemicals

Titanium dioxide (P25) (Acros), iron(III) nitrate nonahydrate ($Fe((NO_3))_3$) (Acros), sulfur (Acros), thioacetamide (TAA) (Acros), N,N-dimethylformamide (DMF) (JT/Macron), ampicillin (Bioshop), glycerol (Honeywell), lysogeny broth (LB) broth miller (Bioshop), LB agar miller (Bioshop), agar-A (Biobasic), 2′,7′-dichlorofluorescin diacetate (DCFH-DA) (Sigma-Aldrich), and Hoechst 33342 (Biotium) were commercially acquired.

Preparation of TiO_2-FeS_2 NCs Onto Carbon Fiber Paper (CFP)

$Fe((NO_3))_3{\cdot}9H_2O$ (8 mmol), thioacetamide (100 mmol), and TiO_2 (8 mmol, P25) were dissolved in 10 mL DMF and then transferred to a Teflon container. The Teflon container was fixed in an autoclave reactor and placed in a hot-air oven (JOV-40) at 180°C for 18 h. After cooling to room temperature, the solution was centrifuged (Heraeus multifuge X1R, Thermo Scientific) at 4000 rpm for 10 min and washed with ethanol to remove excess organic residues. Afterward, the primary product of FeS_2-NCs was collected and dried in the oven. A mixture of the primary product of FeS_2-NCs (0.1 g) and sulfur powder (0.3 g) was placed in a furnace (Thermofisher Lindberg Blue M) at 500°C for 1 h to obtain the final product of TiO_2-FeS_2 NCs. For antibacterial tests, TiO_2 NPs (0.4 mg), FeS_2 NPs (0.4 mg), and TiO_2-FeS_2 NCs (0.8 mg) were, respectively, drop-cast onto CFP (CeTech) with dimensions of 1 x 2 cm.

Structural and Optical Characterizations

SEM (JEOL JSM-7800F) and TEM (Hitachi HT-7700) were carried out to characterize the structures of the materials used in the work such as TiO_2 NPs, FeS_2 NPs, and TiO_2-FeS_2 NCs. To prepare TEM samples, TiO_2 NPs, FeS_2 NPs, and TiO_2-FeS_2 NCs were dispersed in ethanol and then drop-cast onto a copper mesh. After being air-dried, the copper mesh with the materials was used for TEM characterization. XRD studies were carried out using A Rigaku Miniflex 600 with Cu Kα radiation generated at 30 mA and 30 KeV. Scans for XRD were operated from 20° to 70°. Raman data were measured using an Olympus objective Plan N lens at 16 mW. SEM images, TEM images, XRD data, and surface-enhanced Raman spectroscopic (SERS) measurements were used to validate the structural properties of the TiO_2 NPs, FeS_2 NPs and TiO_2-FeS_2 NCs. A UV-Vis-NIR absorption spectrometer (Jasco V-770) was used to detect and validate the optical properties of TiO_2 NPs, FeS_2 NPs, and TiO_2-FeS_2 NCs.

Antibacterial Activity Test

To culture *E. coli*, LB medium was prepared by mixing 5 g of LB broth (Miller) and 1000 mL of sterilized water. *Escherichia coli* (150 µL) was cultured in medium containing of 3 mL of LB medium and 300 µL ampicillin (100 µg/mL) in a shaker at 160 rpm under 37°C for 3 h. The colony-forming unit (CFU) value of the *E. coli* solution was evaluated by the optical density (OD) at a wavelength of 600 nm (OD600). For *E. coli*, OD600 of 1.0 is calculated to be 8×10^8 CFU/mL. In this study, a solution of *E. coli* with an OD600 of 0.1 was utilized for the antibacterial test. For the light-induced antibacterial test, a solar simulator (Enlitech) was used to simulate AM1.5 sunlight. TiO_2 NPs, FeS_2 NPs, and TiO_2-FeS_2 NCs drop-cast onto CFP were immersed in *E. coli* solutions and then TiO_2 NPs, FeS_2 NPs and TiO_2-FeS_2 NCs were irradiated for 3 min with simulated AM1.5 sunlight. After light irradiation, *E. coli* solutions were cultured in a shaker at 160 rpm and 37°C. During culture, the OD600 values of *E. coli* solutions were measured every 30 min. Bacterial growth curves were used to evaluate the antibacterial activities of TiO_2 NPs and TiO_2-FeS_2 NCs under light irradiation.

Analysis of ROS Generation

ROS generation was measured and validated using a 2′,7′-dichlorodihydrofluorescein diacetate (H2DCFDA) assay. For the H2DCFDA assay, H2DCFDA can be oxidized by ROS into 2′,7′-dichlorofluorescein (DCF). DCF is highly fluorescent and can be measured by fluorescence spectroscopy with excitation/emission at 488/525 nm. The fluorescence intensity of DCF revealed the total amount of ROS production. Furthermore, the dye of Hoechst 33,342 was applied to measure the total amount of bacteria. The fluorescence intensity of Hoechst 33,342 with excitation/emission at 350/461 nm wavelengths showed the total amount of bacteria. For the analysis of ROS generation, in brief, 10 µM of DCFH-DA and 1 µg/mL of Hoechst 33,342 were separately added to *E. coli* culture medium in a 96-well plate. Afterward, *E. coli* solutions were incubated at 37°C and 200 rpm for 20 min. After incubation, *E. coli* solutions were centrifuged at 10^4 *g* for 2 min, and the supernatants were removed. Precipitates were suspended in sterilized water. The washing procedures were repeated once. The fluorescence intensities of DCF (excitation/emission wavelength at 488/525 nm) and Hoechst 33342 (excitation/emission wavelength at 350/461 nm) were measured on a microplate reader (Thermo Varioskan Flash). For the different numbers of *E. coli* in different experiments, the total amount of ROS was normalized to the total bacterial number. The relative ROS level was calculated by normalizing the ROS level between the experimental group and the control group.

Results and Discussion

Morphological Characterization

The morphologies of TiO_2 NPs, FeS_2 NPs, and TiO_2-FeS_2 NCs were first characterized by SEM as shown in Figure 1A-C, respectively. In the SEM image of Figure 1A, TiO_2 NPs (P25) exhibited a spherical shape and revealed the formation of aggregates. For FeS_2 NPs and TiO_2-FeS_2 NCs, globular aggregates were observed as shown in Figure 1B and C. To further characterize their structures, TiO_2 NPs, FeS_2 NPs, and TiO_2-FeS_2 NCs were examined by TEM as, respectively, shown in Figure 1D-F. As shown in the TEM image of Figure 1D, TiO_2 NPs clearly revealed a spherical shape with an average size of 25 nm. In Figure 1E, FeS_2 NPs exhibited slight aggregates. The blue arrow indicates FeS_2 NPs in Figure 1E. Most importantly, as shown in the TEM image of Figure 1F, TiO_2-FeS_2 NCs exhibited heterostructures composed by TiO_2 NPs (red arrow) and FeS_2 NPs (blue arrow). High-resolution transmission electron microscopy image of heterostructured TiO_2-FeS_2 NCs was shown in the supporting information of Figure S1. Moreover, the energy-dispersive X-ray spectroscopy (EDS) was applied to measure weight percentages of FeS_2 and TiO_2 in TiO_2-FeS_2 NCs. In the supporting information of Figure S2, EDS spectra showed that weight percentages of FeS_2 and TiO_2 in TiO_2-FeS_2 NCs were, respectively, 49.47% and 50.53%. Overall, SEM images, TEM images, and EDS spectra demonstrated the successful preparation of TiO_2 NPs, FeS_2 NPs and TiO_2-FeS_2 NCs for subsequent antibacterial applications.

Structural Analysis of TiO_2-FeS_2 NCs

XRD was utilized to investigate the crystal structure of TiO_2-FeS_2 NCs. In Figure 2, clear XRD peaks at 25.4°, 37.8°, 48.0°, and 54.5° were accordingly cataloged to the (101), (004), (200) and, (211) planes of the anatase phase of TiO_2 (JCPDS 21–1272), and XRD peaks at 27.5° and, 54.4° were accordingly cataloged to the (110) and (211) planes of the rutile phase of TiO_2 (JCPDS 21–1276). XRD peaks of FeS_2 NPs were matched with approved pyrite FeS_2 (JCPDS

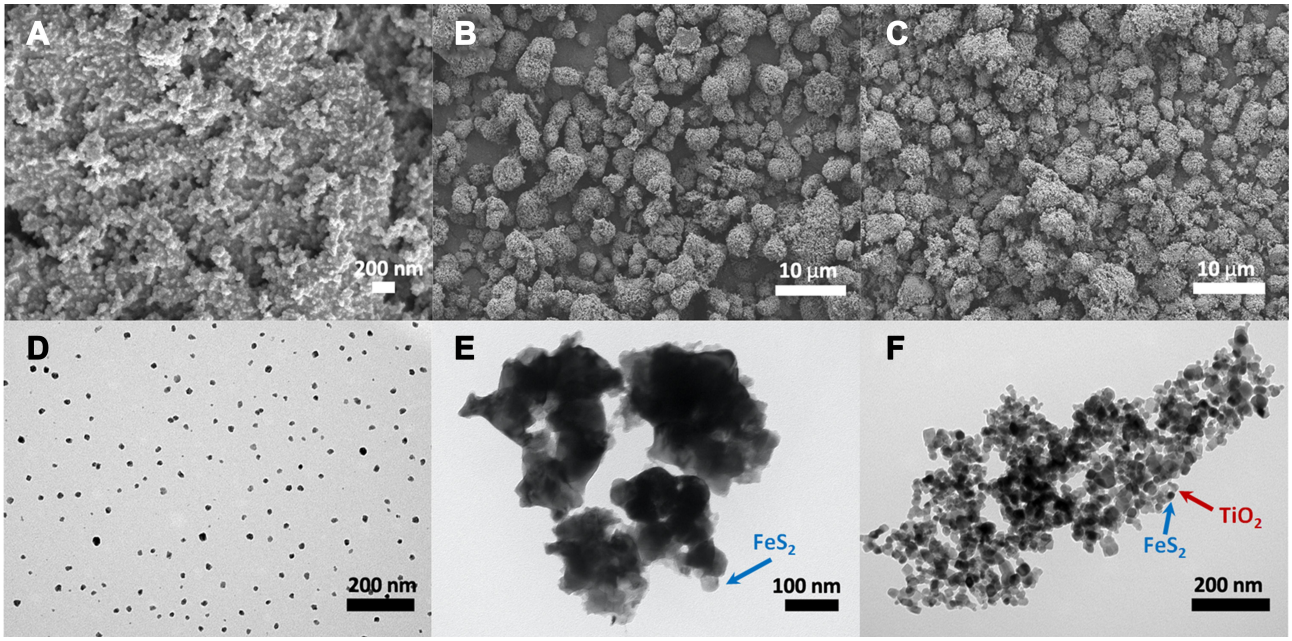

Figure 1 SEM images of (**A**) TiO_2 NPs, (**B**) FeS_2 NPs and (**C**) TiO_2-FeS_2 NCs. TEM Images of (**D**) TiO_2 NPs, (**E**) FeS_2 NPs and (**F**) TiO_2-FeS_2 NCs. The blue arrow indicated FeS_2 NPs and the red arrow indicated TiO_2 NPs.
Abbreviations: SEM, scanning electron microscopy; TiO_2, titanium dioxide; FeS_2, iron disulfide; NPs, nanoparticles; NCs, nanocomposites; TEM, transmission electron microscopy.

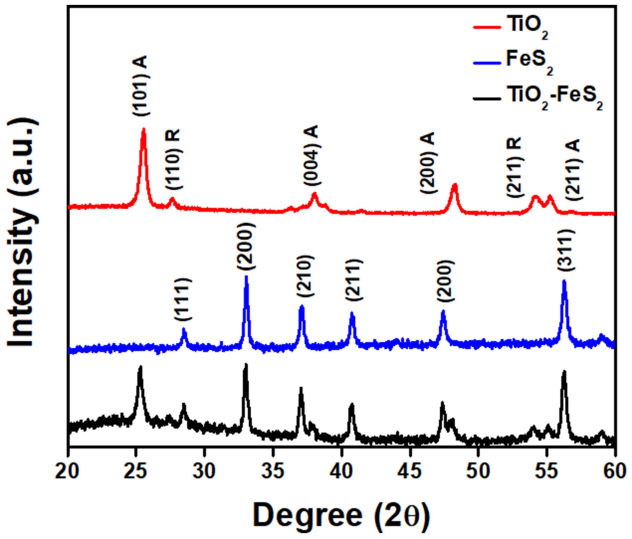

Figure 2 XRD spectra of TiO_2 NPs, FeS_2 NPs, and TiO_2-FeS_2 NCs. (A: anatase; R: rutile).
Abbreviations: XRD, powder x-ray diffraction; TiO_2, titanium dioxide; NPs, nanoparticles; FeS_2, iron disulfide; NCs, nanocomposites.

42–1340). The principal peaks of FeS_2 NPs at 28.5°, 33.1°, 37.1°, 40.8°, 47.4°, and 56.3° were accordingly cataloged to the (111), (200), (210), (211), (220), and (311) planes of pyrite FeS_2 as shown in Figure 2. Results of XRD studies also revealed the crystalline nature of TiO_2-FeS_2 NCs. To sum up, TiO_2-FeS_2 NCs were composed of TiO_2 NPs and FeS_2 NPs according to SEM and TEM measurements.

Furthermore, Raman spectra of TiO_2 NPs, FeS_2 NPs, and TiO_2-FeS_2 NCs were studied to evaluate and validate their structural properties and confirm the formation of TiO_2-FeS_2 NCs. As shown in Figure 3, Raman frequencies of TiO_2 NPs were 143 (E_g), 395 (B_{1g}), 513 (B_{1g}), and 633 cm^{-1} (E_g) for the TiO_2 anatase phase. For FeS_2 NPs, there were two strong peaks located at 338 (E_g) and 377 cm^{-1} (A_g) corresponding to pyrite FeS_2.[37] The two weak Raman signals of 220 and 283 cm^{-1} were attributed to the presence of FeS due to sulfur insufficiency and sulfur vacancies.[38,39] For Raman spectra of TiO_2-FeS_2 NCs, the peak at 143 cm^{-1} was attributed to the Raman signal of TiO_2 NPs (E_g), and the two peaks at 338 and 373 cm^{-1} were, respectively, attributed to Raman signals of E_g and A_g of FeS_2 NPs. Based on the results of Raman spectra, TiO_2-FeS_2 NCs were composed of TiO_2 NPs and FeS_2 NPs. Based on examination of SEM images, TEM images, XRD spectra, and Raman spectra, TiO_2-FeS_2 NCs were successfully prepared by a simple solution process.

Optical Properties of TiO_2-FeS_2 NCs

UV-Vis-NIR spectra were used to investigate the optical properties of TiO_2 NPs, FeS_2 NPs, and TiO_2-FeS_2 NCs. In UV-Vis-NIR spectra of Figure 4, absorption curves of TiO_2 NPs, FeS_2 NPs and TiO_2-FeS_2 NCs are depicted. Photoactivitiesof TiO_2 NPs were only found in the UV region of the electromagnetic spectrum. Bandgaps of

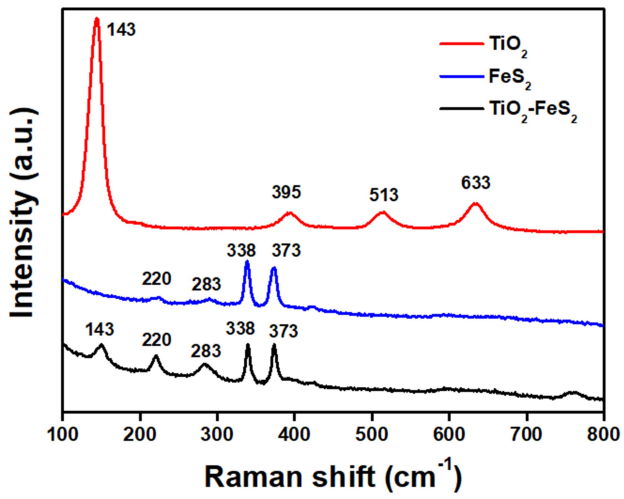

Figure 3 Raman spectra of TiO_2 NPs, FeS_2 NPs, and TiO_2-FeS_2 NCs.
Abbreviations: TiO_2, titanium dioxide; NPs, nanoparticles; FeS_2, iron disulfide; NCs, nanocomposites.

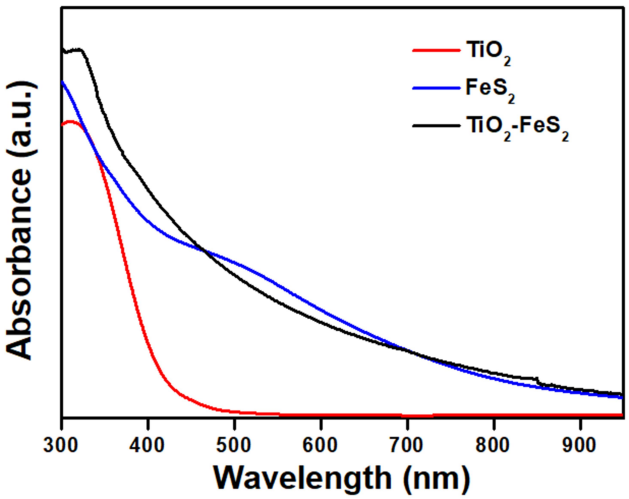

Figure 4 UV-Vis-NIR spectra of TiO_2 NPs, FeS_2 NPs, and TiO_2-FeS_2 NCs.
Abbreviations: UV-Vis-NIR, ultraviolet-visible-near-infrared; TiO_2, titanium dioxide; NPs, nanoparticles; FeS_2, iron disulfide; NCs, nanocomposites.

TiO_2 (anatase) and TiO_2 (rutile) were, respectively, found to be 3.2 and 3.0 eV according to their absorption wavelengths at 388 and 413 nm. Therefore, the absorption spectra of TiO_2 NPs suddenly decreased after 413 nm.[40] FeS_2 NPs were seen to have absorption in a wide range from Vis to NIR due to their band gap of 0.95 eV. The absorption of TiO_2-FeS_2 NCs was clearly observed from UV to NIR because of the combination of the absorption curves of TiO_2 NPs and FeS_2 NPs.[41] Results of UV-Vis-NIR spectra indicated that the absorption of TiO_2-FeS_2 NCs was extended from UV to NIR compared to that of TiO_2 NPs.

Light-Induced Antibacterial Activity of TiO_2-FeS_2 NCs

To investigate light-induced antibacterial activities, TiO_2 NPs, FeS_2 NPs, and TiO_2-FeS_2 NCs incubated with *E. coli* solutions were irradiated with simulated AM1.5 sunlight and not irradiated. After light irradiation for 3 min, the OD600 value of the *E. coli* solution was found to be 0.85 after culturing for 150 min as shown in the growth curve (green line) of Figure 5A. Without light irradiation, the growth curve of *E. coli* showed no significant change compared to that of *E. coli* with light irradiation for 3 min. To investigate the light-induced antibacterial activity, TiO_2 NPs, FeS_2 NPs, and TiO_2-FeS_2 NCs were incubated with *E. coli* solutions and then irradiated with light for 3 min. As shown in the growth curves of Figure 5A, after light irradiation for 3 min, OD600 values of *E. coli* solutions incubated with TiO_2 NPs (red line), FeS_2 NPs (blue line), and TiO_2-FeS_2 NCs (black line) were, respectively, 0.52, 0.58, and 0.49 after culturing for 150 min. Bacterial growth results indicated that light-induced antibacterial activities increased in the order of FeS_2 NPs, TiO_2 NPs, and TiO_2-FeS_2 NCs. To further examine the light-harvesting capability of FeS_2 NPs in TiO_2-FeS_2 NCs, a 515-nm longpass filter was applied to exclude light wavelengths shorter than 515 nm. As shown in Figure 5A and B, under light irradiation, growth curves of *E. coli* revealed no changes with and without the 515-nm longpass filter. However, with the 515-nm longpass filter, light-induced antibacterial activities of TiO_2 NPs, FeS_2 NPs, and TiO_2-FeS_2 NCs all decreased, as shown in Figure 5B. After light irradiation for 3 min with the 515-nm longpass filter, OD600 values of *E. coli* solutions incubated with TiO_2 NPs (red line), FeS_2 NPs (blue line), and TiO_2-FeS_2 NCs (black line) were, respectively, 0.85, 0.79, and 0.67 after culturing for 150 min. Obviously, with the 515-nm longpass filter, light absorption by TiO_2 NPs was cut off, resulting in no light-induced antibacterial activity. For FeS_2 NPs, the light-induced antibacterial activity was still exhibited because FeS_2 NPs can absorb light wavelengths longer than 515 nm. Moreover, with the light harvester of FeS_2 NPs, the light-induced antibacterial activity of TiO_2-FeS_2 NCs was retained with the use of the 515-nm longpass filter. When using the filter to restrict light wavelengths shorter than 515 nm, the light-induced antibacterial activity of TiO_2-FeS_2 NCs could be attributed to that the light harvester of FeS_2 NPs in the TiO_2-FeS_2 NCs, which could absorb light wavelengths

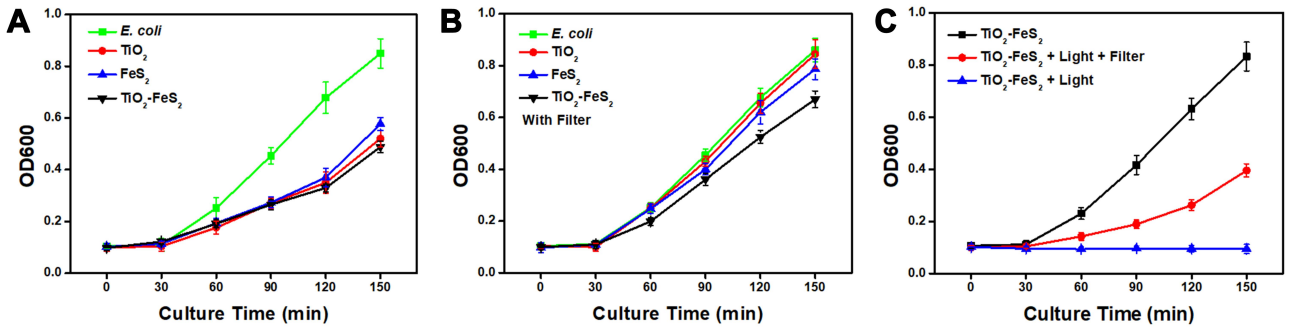

Figure 5 Growth curves of *E. coli* (optical density, OD 600 nm) of (**A**) *E. coli* only and with TiO_2 NPs, FeS_2 NPs, and TiO_2-FeS_2 NCs under light irradiation for 3 min, (**B**) *E. coli* only and with TiO_2 NPs, FeS_2 NPs, and TiO_2-FeS_2 NCs under light irradiation for 3 min with a 515-nm longpass filter, (**C**) TiO_2-FeS_2 NCs without light irradiation (black line), TiO_2-FeS_2 NCs under light irradiation for 30 min with a 515-nm longpass filter (red line), and TiO_2-FeS_2 NCs under light irradiation for 30 min (blue line). All data presented as means ± SD, n=3 per group.
Abbreviations: *E. coli, Escherichia coli*; TiO_2, titanium dioxide; NPs, nanoparticles; FeS_2, iron disulfide; NCs, nanocomposites.

longer than 515 nm to generate photoinduced electrons, and then those photoelectrons were transferred to TiO_2 NPs to generate ROS. Furthermore, after light irradiation for 30 min with the 515-nm longpass filter, the final OD600 value of *E. coli* incubated with TiO_2-FeS_2 NCs was found to be 0.39 as shown in Figure 5C. Without light irradiation, the final OD600 value of *E. coli* incubated with TiO_2-FeS_2 NCs was 0.83. Most importantly, after light irradiation for 30 min, there was no growth of *E. coli* in the presence of TiO_2-FeS_2 NCs as a light-activated antibacterial agent. Overall, results of light-induced antibacterial activity suggested that with TiO_2-FeS_2 NCs, FeS_2 NPs acted as a superior light harvester to absorb light in the Vis and NIR regions to generate photoelectrons, and then the photoelectrons were delivered from FeS_2 NPs to TiO_2 NPs for improved ROS generation.

Investigation of ROS Generation

TiO_2-based materials were found to possess remarkable antibacterial activities due to ROS generation under UV light irradiation.[42–44] Therefore, to investigate antibacterial activities, ROS generation activities of TiO_2 NPs, FeS_2 NPs, and TiO_2-FeS_2 NCs incubated with *E. coli* were measured by an H2DCFDA assay with and without light irradiation. In Figure 6, for the control experiment, the ROS level of *E. coli* without light irradiation was set to 1.0. Compared to *E. coli* with light irradiation for 3 min, the relative ROS level revealed no significant change due to no light-induced antibacterial agent being produced. Moreover, without light irradiation, neither TiO_2 NPs, FeS_2 NPs, nor TiO_2-FeS_2 NCs showed any obvious increases in ROS. With light irradiation for 3 min, relative ROS levels of TiO_2 NPs, FeS_2 NPs, and TiO_2-FeS_2 NCs were, respectively, 2.51-, 1.88-, and 3.34-fold higher compared to that of the control experiment. However, under light irradiation with a 515-nm longpass filter, relative ROS levels of TiO_2 NPs, FeS_2 NPs, and TiO_2-FeS_2 NCs were, respectively, 1.13-, 1.43-, and 1.63-fold higher compared to that of the control experiment. For TiO_2 NPs with light irradiation, relative ROS levels dramatically decreased from 2.51-fold (without the filter) to 1.13-fold (with the filter) because the light absorption of TiO_2 NPs was reduced by the filter. For FeS_2 NPs under light irradiation, relative ROS levels only dropped from 1.88-fold (without) to 1.13-fold (with the filter). The reason

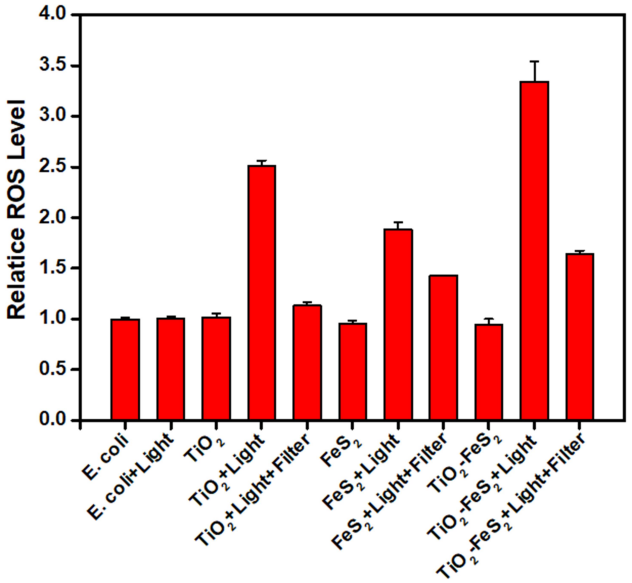

Figure 6 ROS levels of *E. coli* without light irradiation was set to 1.0. Relative ROS levels of *E. coli* after incubation with TiO_2 NPs, FeS_2 NPs, and TiO_2-FeS_2 NCs with and without light irradiation and a 515-nm filter, respectively. All data presented as means ± SD, n=3 per group.
Abbreviations: ROS, reactive oxygen species; *E. coli, Escherichia coli*; TiO_2, titanium dioxide; NPs, nanoparticles; FeS_2, iron disulfide; NCs, nanocomposites.

can be attributed to FeS_2 NPs still being able to absorb light at wavelengths longer than 515 nm to produce photoelectrons for ROS generation. For TiO_2-FeS_2 NCs, relative ROS levels decreased from 3.34- (with light irradiation) to 1.64-fold (with light irradiation and the filter). Under light irradiation with the 515-nm filter, the light-induced antibacterial activity of TiO_2-FeS_2 NCs suggested that photoelectrons generated by FeS_2 NPs in TiO_2-FeS_2 NCs were transferred to the conduction band of TiO_2 NPs to generate more ROS (1.63-fold) compared to that of only FeS_2 NPs (1.43-fold). For TiO_2 NPs, FeS_2 NPs, and TiO_2-FeS_2 NCs, results of the ROS tests were consistent with measurements of antibacterial activities.

To further examine the effect of ROS, the morphologies of *E. coli* incubated with TiO_2-FeS_2 NCs before and after light irradiation were characterized by SEM. As shown in Figure 7A, after incubation with TiO_2-FeS_2 NCs, *E. coli* revealed compact membrane structure without light irradiation. However, with light irradiation for 3 min, *E. coli* incubation with TiO_2-FeS_2 NCs appeared slight membrane rupture as indicated by the yellow arrows in Figure 7B. Furthermore, the complete rupture of *E. coli* membrane was observed as indicated by the white arrows. In high-resolution SEM image of Figure 7C, the slight membrane rupture and complete rupture of *E. coli* membrane were respectively indicated by the yellow arrow and the white arrows. The results indicated that in the system of TiO_2-FeS_2 NCs, under light irradiation, the increases of ROS generation enhanced for the destruction of bacterial membrane.[45–47]

Mechanism of Light-Induced Antibacterial Activity of TiO_2-FeS_2 NCs

Bandgaps of TiO_2 NPs and FeS_2 NPs were, respectively, found to be 3.2 and 0.95 eV in the UV-Vis-NIR region of the electromagnetic spectrum. The combination of TiO_2 NPs and FeS_2 NPs was demonstrated to have increased photoactivity. Herein, TiO_2-FeS_2 NCs were also demonstrated to have superior light-induced antibacterial activity compared to that of only TiO_2 NPs or only FeS_2 NPs. A schematic of the mechanism of light-induced antibacterial activity of TiO_2-FeS_2 NCs is shown in Figure 8. With reference to the normal hydrogen electrode (NHE), values of the conduction band (CB) and valence band (VB) of TiO_2 NPs were −0.2 and 3 eV, respectively. Therefore, TiO_2 NPs can absorb UV light to generate photoinduced electrons and holes for ROS production, including $\cdot O_2^-$ (−0.16 eV) and ·OH (2.32 eV). For FeS_2 NPs, CB and VB were, respectively, −0.5 and 0.45 eV. In TiO_2-FeS_2 NCs, FeS_2 NPs acted as light harvesters to absorb light from Vis to NIR to produce photoinduced electrons and holes. Furthermore, the photoinduced electrons in the CB of FeS_2 NPs were transferred to the CB of TiO_2 NPs to facilitate ROS generation. Overall, the light-induced antibacterial activity of TiO_2-FeS_2 NCs was enhanced by the light harvesters of FeS_2 NPs due to the broad range of light absorption from UV to NIR.

Conclusions

TiO_2-FeS_2 NCs were successfully synthesized by a simple solution process, and their structural and optical properties were validated by SEM, TEM, XRD, Raman spectroscopy, and UV-Vis-NIR spectroscopy. TiO_2-FeS_2 NCs exhibited a broad range of light absorption from UV to NIR, because of the combination of the absorptions of TiO_2 NPs and FeS_2 NPs. In TiO_2-FeS_2 NCs, FeS_2 NPs acted as a superior light harvester to increase light absorption from the Vis and NIR ranges. With light irradiation for 3 min, OD600 values of *E. coli* solutions incubated with TiO_2 NPs, FeS_2 NPs, and TiO_2-FeS_2 NCs were, respectively, 0.52, 0.58, and 0.49 after culturing for 150 min, indicating that the best antibacterial activity was with TiO_2-FeS_2 NCs. Light-induced antibacterial

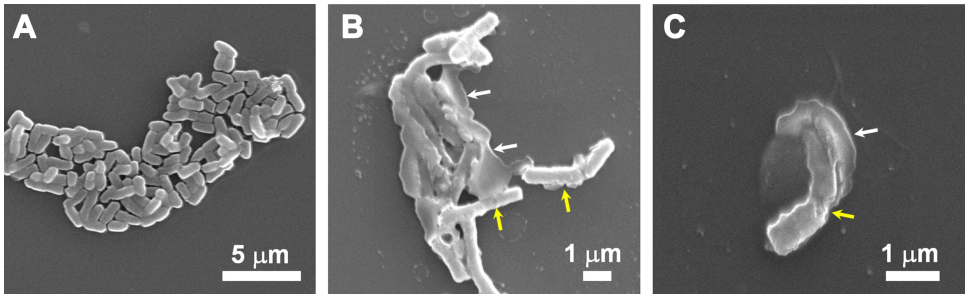

Figure 7 SEM images of (**A**) *E. coli* incubated with TiO_2-FeS_2 NCs before light irradiation and (**B**) *E. coli* incubated with TiO_2-FeS_2 NCs after light irradiation. (**C**) High-resolution SEM image of *E. coli* with clear membrane rupture. The yellow arrows indicated the membrane rupture of *E. coli*. The white arrows indicated the complete rupture of *E. coli* membrane.

Abbreviations: SEM, scanning electron microscopy; *E. coli, Escherichia coli*; TiO_2, titanium dioxide; FeS_2, iron disulfide; NCs, nanocomposites.

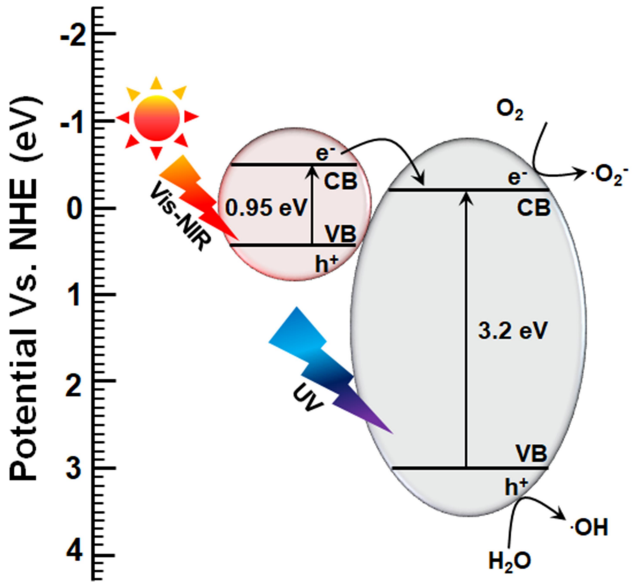

Figure 8 Schematic illustration of the transfer of photoinduced electrons from FeS_2 NPs to TiO_2 NPs in TiO_2-FeS_2 NCs for ROS generation under ultraviolet, visible, and near infrared light illumination.
Abbreviations: FeS_2, iron disulfide; NPs, nanoparticles; TiO_2, titanium dioxide; NCs, nanocomposites; ROS, reactive oxygen species.

activities of FeS_2 NPs, TiO_2 NPs, and TiO_2-FeS_2 NCs can be attributed to ROS generation. Under light irradiation, relative ROS levels increased in the decreasing order of FeS_2 NPs (1.88-fold), TiO_2 NPs (2.51-fold), and TiO_2-FeS_2 NCs (3.34-fold). In TiO_2-FeS_2 NCs, TiO_2 NPs absorbed UV light to generate photoinduced electrons and holes for ROS generation, including $\cdot O_2^-$ and ·OH. Furthermore, FeS_2 NPs in TiO_2-FeS_2 NCs harvested the light from Vis to NIR to produce photoinduced electrons, and then the photoinduced electrons from FeS_2 NPs were transferred to TiO_2 NPs to facilitate ROS generation. Our work demonstrated that TiO_2-FeS_2 NCs with superior light-induced antibacterial activity could be a potential antibacterial agent for future antibacterial applications in fields such as medicine, food, and water quality.

Acknowledgments

This work was financially supported by MOST109-2636-E-038-001, MOST 109-2113-M-038-005-MY2, Taipei Medical University and the Higher Education Sprout Project by the Ministry of Education (MOE) in Taiwan. We would like to acknowledge Yuan-Chin Hsiung, Chun-Chih Liu and Dr. Chi-Ming Lee for her/his excellent technical support at the TMU Core Facility Center.

Disclosure

The authors declare no conflicts of interest.

References

1. Mutalik C, Wang D-Y, Krisnawati DI, Jazidie A, Yougbare S, Kuo T-R. Light-activated heterostructured nanomaterials for antibacterial applications. *Nanomaterials*. 2020;10(4):643. doi:10.3390/nano10040643
2. Luo J, Deng W, Yang F, Wu Z, Huang M, Gu M. Gold nanoparticles decorated graphene oxide/nanocellulose paper for NIR laser-induced photothermal ablation of pathogenic bacteria. *Carbohydr Polym*. 2018;198:206–214. doi:10.1016/j.carbpol.2018.06.074
3. Teng CP, Zhou T, Ye E, et al. Effective targeted photothermal ablation of multidrug resistant bacteria and their biofilms with NIR-absorbing gold nanocrosses. *Adv Healthcare Mater*. 2016;5:2122–2130. doi:10.1002/adhm.201600346
4. Khan SA, Singh AK, Senapati D, Fan Z, Ray PC. Bio-conjugated popcorn shaped gold nanoparticles for targeted photothermal killing of multiple drug resistant salmonella Dt104. *J Mater Chem*. 2011;21:17705–17709. doi:10.1039/c1jm13320a
5. de Kraker ME, Stewardson AJ, Harbarth S. Will 10 million people die a year due to antimicrobial resistance by 2050? *PLoS Med*. 2016;13(11):e1002184. doi:10.1371/journal.pmed.1002184
6. Matsunaga T, Tomoda R, Nakajima T, Wake H. Photoelectrochemical sterilization of microbial cells by semiconductor powders. *FEMS Microbiol Lett*. 1985;29:211–214. doi:10.1111/j.1574-6968.1985.tb00864.x
7. Mills A, Le Hunte S. An overview of semiconductor photocatalysis. *J Photochem Photobiol A Chem*. 1997;108:1–35. doi:10.1016/S1010-6030(97)00118-4
8. Nadtochenko V, Denisov N, Sarkisov O, Gumy D, Pulgarin C, Kiwi J. Laser kinetic spectroscopy of the interfacial charge transfer between membrane cell walls of E. Coli and TiO_2. *J Photochem Photobiol A Chem*. 2006;181:401–407. doi:10.1016/j.jphotochem.2005.12.028
9. Caratto V, Ball L, Sanguineti E, et al. Antibacterial activity of standard and n-doped titanium dioxide-coated endotracheal tubes: an in vitro study. *Revista Brasileira De Terapia Intensiva*. 2017;29:55–62. doi:10.5935/0103-507X.20170009
10. Kangwansupamonkon W, Lauruengtana V, Surassmo S, Ruktanonchai U. Antibacterial effect of apatite-coated titanium dioxide for textiles applications. *Nanomedicine*. 2009;5:240–249. doi:10.1016/j.nano.2008.09.004
11. Deepagan V, You DG, Um W, et al. Long-Circulating Au-TiO_2 nanocomposite as a sonosensitizer for ROS-mediated eradication of cancer. *Nano Lett*. 2016;16:6257–6264. doi:10.1021/acs.nanolett.6b02547
12. Liu R, Wang X, Ye J, et al. Enhanced antibacterial activity of silver-decorated sandwich-like mesoporous silica/reduced graphene oxide nanosheets through photothermal effect. *Nanotechnology*. 2018;29:105704. doi:10.1088/1361-6528/aaa624
13. Prakash J, Sun S, Swart HC, Gupta RK. Noble metals-TiO_2 nanocomposites: from fundamental mechanisms to photocatalysis, surface enhanced Raman scattering and antibacterial applications. *Appl Mater Today*. 2018;11:82–135. doi:10.1016/j.apmt.2018.02.002
14. Hamzah MQ, Mezan SO, Tuama AN, Jabbar AH, Agam MA. Study and characterization of polystyrene/titanium dioxide nanocomposites (PS/TiO_2 NCS) for photocatalytic degradation application: a review. *Int J Eng Technol*. 2018;7:538–543. doi:10.14419/ijet.v7i4.30.28172
15. Nabiyouni G, Ghanbari D. Simple preparation of magnetic, antibacterial and photo-catalyst Nife2o4@ TiO_2/Pt nanocomposites. *J Nanostruct*. 2018;8:408–416.
16. Tang S, Wang Z, Li P, et al. Degradable and photocatalytic antibacterial Au-TiO_2/Sodium alginate nanocomposite films for active food packaging. *Nanomaterials*. 2018;8:930. doi:10.3390/nano8110930
17. Mathew S, Ganguly P, Rhatigan S, et al. Cu-doped TiO_2: visible light assisted photocatalytic antimicrobial activity. *Appl Sci*. 2018;8:2067. doi:10.3390/app8112067

18. Kőrösi L, Bognár B, Horváth M, et al. Hydrothermal evolution of PF-Co-doped TiO_2 nanoparticles and their antibacterial activity against carbapenem-resistant klebsiella pneumoniae. *Appl Catal B*. 2018;231:115–122. doi:10.1016/j.apcatb.2018.03.012
19. Ghilini F, Rodríguez González MC, Miñán AG, et al. Highly stabilized nanoparticles on poly-L-lysine-coated oxidized metals: a versatile platform with enhanced antimicrobial activity. *ACS Appl Mater Interfaces*. 2018;10:23657–23666. doi:10.1021/acsami.8b07529
20. Huang S-M, Weng C-H, Tzeng J-H, et al. Photocatalytic inactivation of Klebsiella Pneumoniae by visible-light-responsive N/C-Doped and N-Tourmaline/Palladium-C-Codoped TiO_2. *Chem Eng J*. 2020;379:122345. doi:10.1016/j.cej.2019.122345
21. Meekins BH, Kamat PV. Got TiO_2 nanotubes? Lithium ion intercalation can boost their photoelectrochemical performance. *ACS Nano*. 2009;3:3437–3446. doi:10.1021/nn900897r
22. Sivakami R, Thiyagarajan P. Synthesis and luminescence properties of Zns: ce3+, Li+, Mn2+ nanophosphors. *Nano Struct Nano Objects*. 2016;6:59–66. doi:10.1016/j.nanoso.2016.03.001
23. Asahi R, Morikawa T, Irie H, Ohwaki T. Nitrogen-doped titanium dioxide as visible-light-sensitive photocatalyst: designs, developments, and prospects. *Chem Rev*. 2014;114:9824–9852. doi:10.1021/cr5000738
24. Ananpattarachai J, Seraphin S, Kajitvichyanukul P. Formation of hydroxyl radicals and kinetic study of 2-chlorophenol photocatalytic oxidation using C-Doped TiO_2, N-Doped TiO_2, and C, N Co-Doped TiO_2 under visible light. *Environ Sci Poll Res*. 2016;23:3884–3896. doi:10.1007/s11356-015-5570-8
25. Ismail AA, Kandiel TA, Bahnemann DW. Novel (and better?) titania-based photocatalysts: brookite nanorods and mesoporous structures. *J Photochem Photobiol A Chem*. 2010;216:183–193. doi:10.1016/j.jphotochem.2010.05.016
26. Ksibi M, Rossignol S, Tatibouët J-M, Trapalis C. Synthesis and solid characterization of nitrogen and sulfur-doped TiO_2 photocatalysts active under near visible light. *Mater Lett*. 2008;62:4204–4206. doi:10.1016/j.matlet.2008.06.026
27. Li L, Yang Y, Liu X, et al. Synthesis of B-doped TiO_2 and its photocatalytic performance on degradation of RHB. *Appl Surf Sci*. 2013;265:36–40. doi:10.1016/j.apsusc.2012.10.075
28. Nainani R, Thakur P, Chaskar M. Synthesis of silver doped TiO_2 nanoparticles for the improved photocatalytic degradation of methyl orange. *J Mater Sci Eng B*. 2012;2:52–58.
29. Pal NK, Kryschi C. Improved photocatalytic activity of gold decorated differently doped TiO_2 nanoparticles: a comparative study. *Chemosphere*. 2016;144:1655–1664. doi:10.1016/j.chemosphere.2015.10.060
30. Sadeghi-Niaraki S, Ghasemi B, Habibolahzadeh A, Ghasemi E, Ghahari M. Nanostructured Fe_2O_3@ TiO_2 pigments with improved NIR reflectance and photocatalytic ability. *Mater Chem Phys*. 2019;121769. doi:10.1016/j.matchemphys.2019.121769
31. Yan D, Wu X, Pei J, Wu C, Wang X, Zhao H. Construction of G-C3n4/Tio2/Ag composites with enhanced visible-light photocatalytic activity and antibacterial properties. *Ceramics Int*. 2020;46:696–702. doi:10.1016/j.ceramint.2019.09.022
32. Siwińska-Stefańska K, Kubiak A, Piasecki A, et al. Hydrothermal synthesis of multifunctional TiO_2-Zno oxide systems with desired antibacterial and photocatalytic properties. *Appl Surf Sci*. 2019;463:791–801. doi:10.1016/j.apsusc.2018.08.256
33. Fang JH, Wu JW, Su LY, Zhang XY, Lu ZH. Modification of TiO_2 microporous electrode with quantum-sized FeS_2 particles. *Chem Lett*. 1997;26:149–150. doi:10.1246/cl.1997.149
34. Xin Y, Li Z, Wu W, Fu B, Zhang Z. Pyrite FeS_2 sensitized TiO_2 nanotube photoanode for boosting near-infrared light photoelectrochemical water splitting. *ACS Sustain Chem Eng*. 2016;4:6659–6667. doi:10.1021/acssuschemeng.6b01533
35. Han E, Hu F, Zhang S, et al. Worm-like FeS_2/TiO_2 nanotubes for photoelectrocatalytic reduction of CO_2 to methanol under visible light. *Energy Fuels*. 2018;32:4357–4363. doi:10.1021/acs.energyfuels.7b03234
36. Kuo T-R, Liao H-J, Chen Y-T, et al. Extended visible to near-infrared harvesting of earth-abundant FeS_2–TiO_2 heterostructures for highly active photocatalytic hydrogen evolution. *Green Chem*. 2018;20:1640–1647. doi:10.1039/C7GC03173D
37. Chang CC, Li SR, Chou HL, et al. Photoactive earth-abundant iron pyrite catalysts for electrocatalytic nitrogen reduction reaction. *Small*. 2019;15:1904723. doi:10.1002/smll.201904723
38. Balachandran U, Eror N. Raman spectra of titanium dioxide. *J Solid State Chem*. 1982;42:276–282. doi:10.1016/0022-4596(82)90006-8
39. Wang D-Y, Li C-H, Li -S-S, et al. Iron Pyrite/Titanium dioxide photoanode for extended near infrared light harvesting in a photoelectrochemical cell. *Sci Rep*. 2016;6:20397. doi:10.1038/srep20397
40. Li X, Wang D, Cheng G, Luo Q, An J, Wang Y. Preparation of polyaniline-modified TiO_2 nanoparticles and their photocatalytic activity under visible light illumination. *Appl Catal B*. 2008;81:267–273. doi:10.1016/j.apcatb.2007.12.022
41. Wang DY, Jiang YT, Lin CC, et al. Solution-processable Pyrite FeS_2 nanocrystals for the fabrication of heterojunction photodiodes with visible to NIR photodetection. *Adv Mater*. 2012;24:3415–3420. doi:10.1002/adma.201200753
42. Ma S, Zhan S, Jia Y, Zhou Q. Superior antibacterial activity of Fe_3O_4 -TiO_2 nanosheets under solar light. *ACS Appl Mater Interfaces*. 2015;7:21875–21883.
43. Li H, Zhong J, Zhu H, et al. Hybrid Cu_2o/TiO_2 nanocomposites with enhanced photocatalytic antibacterial activity toward acinetobacter baumannii. *ACS Appl Bio Mater*. 2019;2:4892–4903. doi:10.1021/acsabm.9b00644
44. Akhavan O. Lasting antibacterial activities of Ag–TiO_2/Ag/a-TiO_2 nanocomposite thin film photocatalysts under solar light irradiation. *J Colloid Interface Sci*. 2009;336:117–124. doi:10.1016/j.jcis.2009.03.018
45. Su H-L, Chou -C-C, Hung D-J, et al. The disruption of bacterial membrane integrity through ROS generation induced by nanohybrids of silver and clay. *Biomaterials*. 2009;30:5979–5987. doi:10.1016/j.biomaterials.2009.07.030
46. Xiang Y, Mao C, Liu X, et al. Rapid and superior bacteria killing of carbon quantum dots/ZNO decorated injectable folic acid-conjugated PDA hydrogel through dual-light triggered ROS and membrane permeability. *Small*. 2019;15:1900322. doi:10.1002/smll.201900322
47. Wang B, Zhang H, An J, et al. Sequential intercellular delivery nanosystem for enhancing ROS-induced antitumor therapy. *Nano Lett*. 2019;19:3505–3518. doi:10.1021/acs.nanolett.9b00336